J Intell Robot Syst (2017) 88:19–35
DOI 10.1007/s10846-017-0532-7

Hexapod Adaptive Gait Inspired by Human Behavior for Six-Legged Robot Without Force Sensor

Yilin Xu · Feng Gao · Yang Pan · Xun Chai

Received: 17 June 2016 / Accepted: 8 March 2017 / Published online: 2 April 2017

Abstract Legged robots are usually installed with force sensors in order to negotiate with the uneven ground. To eliminate the risk of force sensor failure, adaptive gaits integrating indirect force-estimation are of great importance. Robot Octopus III is a robot designed for carrying a payload in the harsh environment. There is no electric device installed on the lower limb of the robot. The indirect force-estimation method, which is based on its spatial parallel mechanism leg, can estimate the external force exerted on the foot tip. In this paper, an adaptive gait is designed after observing human actions. Experiments are carried out to observe how a human walks through the uneven ground when his/her eyes are covered. A static tripod gait mimics the human behavior during the blind walking. When the foot collides with the obstacle, the robot will adjust the foot's height and try to overcome the obstacle. Just like human blind walking, the robot foot tries different locations before it steps on somewhere. The gait also detects if the robot is facing a ditch too deep to step or an obstacle is too high to step on. The gait is implemented in the real-time control system. Experiments are carried out to validate the proposed gait. The robot walked through the uneven ground with maximum obstacle height of 0.2m successfully. The proposed gait enables the robot without foot tip force sensors to walk through the field with obstacles.

Keywords Hexapod · Adaptive gait · Blind walking · Bio-inspired

1 Introduction

Wheeled locomotion is very efficient on flat ground, but legged locomotion has better adaptability on uneven terrain. There is in fact much uneven terrain not only in the nature world but also in the human resident environment. Much effort has been devoted to legged locomotion to improve the mobility of the robot in these environments. Robots with a different number of legs have been designed and manufactured. Currently, there have been one leg robots, biped robots, quadruped robots, hexapod robots, octopod robots, etc. A variety of gait generation methods have been developed on these robots.

The Zero Moment Point (ZMP) constraint has been widely used in the trajectory generation for biped robots or humanoid robots [1], since biped robots usually have a plantar foot. If the moment about the center of the pressure at the supporting foot of a biped robot is zero, then the robot is stable. Park [2] integrated fuzzy-logic with ZMP trajectory generator. The proposed generator reduced the swing motion of the trunk significantly. Some researchers have also explored

Y. Xu · F. Gao (✉) · Y. Pan · X. Chai
State Key Laboratory of Mechanical System and Vibration, Shanghai Jiao Tong University, Shanghai 200240, China
e-mail: fengg@sjtu.edu.cn

the possibility of applying ZMP on quadruped robots or hexapod robots. Kalakrishan et al. [3] designed a body trajectory optimizer based on ZMP constraint for quadruped robots. The trajectory optimizer was integrated into a control system implemented on the quadruped robot LittleDog. It realized fast quadruped locomotion over rough terrain. Moosavian et al. [4] applied ZMP to check the stability of a hexapod robot during its planned motion. As if [5] used ZMP in the generation of the trajectory of a fault-tolerant adaptive gait for a hexapod robot.

The research in the neuroscience also has affected the robotics. The concept of Central Pattern Generator [6] (CPG) originated from neuroscience. Biological CPGs are the neural networks that generate rhythmic signals to drive cyclic activities such as breathing and walking. These neural networks do not need any patterned input or central control to generate rhythmic motor patterned outputs [7]. However, the output of the CPG are determined by some parameters. Efforts have been devoted to finding appropriate methods to determine the CPG parameters. Inada [8] used a genetic algorithm to search the CPG parameters. Nakamura et al. [9] used standard policy gradient methods to train CPG controller for a biped robot. The evolving of these parameters enabled the robot to adapt to the changing terrain. Chen [10] used CPG to archive smooth transition between different gaits of a hexapod robot. Makarov [11] incorporated CPG with the actuator dynamics on a hexapod robot.

Beside CPG, Neural Network is also a concept originating from neuroscience. The difference is that Neural Network usually requires more input signals for the input layer while CPG only requires simple, low-dimensional input signals [6], and CPG is more of an oscillator. The Neural Network can generate new trajectory which has not appeared in the training process, which brings Neural Network certain robustness. Sabourin [12] has trained CMAC neural networks to control a biped robot. The experiment shown that the robot realized stable dynamic walking although the trajectory was different with the simulation result. In fact, training plays a significant role in the application of Neural Networks [13]. The Neural Networks can be trained on-line [14] or off-line [15]. When off-line training is employed, some researchers use time-consuming optimization methods such as genetic algorithms [16], to produce training data.

The aim of this research is to develop an adaptive gait for the hexapod robot Octopus III. The robot is designed to carry high payload and traverse uneven terrain. Many robots use a variety of sensors to enhance their ability to negotiate with the unconstructed environment. These sensors could be IR sensors, laser scanners, cameras, force sensors, IMUs, etc. In this research, to eliminate the risk of breaking an expensive force sensor, the robot uses indirect force-estimation model [17, 18] to evaluate the external forces applied to the foot-tip. This indirect force-estimation model takes the motor current as the input data. Besides, an IMU is also installed on the robot body to detect the attitude of the robot body.

As the origin of legged locomotion, nature inspires researchers. In this research, a robot walking without computer vision is, to some extent, similar to human blind walking. Thus, experiments are performed to observe how a human traverse uneven ground with eyes covered. Some researches are conducted to find a method that enables the robot to imitate human motion. Inamura et al. [19] has proposed a mathematical model based on hidden Markov model. This model realized motion recognition and motion generation. However, in our research, the robot did not merely regenerate trajectories generated in human blind walking, but actually changed the trajectories according to the obstacles it encountered. The robot faced different obstacles in different experiments. Thus, we examined the human blind walking to find inspirations that can be integrated with the gait generation mechanism, such as reactions to the obstacles, in consequences the way which human moves legs and body. Then, based on these conclusions, the hexapod robot adaptive gait is designed. With the help of this gait, the robot can overcome obstacles.

This paper is organized as follows. In Section 2, the robot Octopus III is described, including hardware, software structure, and mathematic model. Section 3 describes the human blind walking experiments and analyzes the results, exploring the inspirations in hexapod locomotion. In Section 4, an adaptive gait for the hexapod robot is proposed based on the analysis in Section 3. Experiments conducted on the robot are described in Section 5. The experiment results are also provided and discussed. Finally, in Section 6, conclusions of this research work are discussed.

2 Robot Octopus III

2.1 Hardware and Software

Robot Octopus III [20, 21] is a hexapod robot designed for rescue tasks performed in a nuclear power plant. Figure 1 is a photo of the robot. Figure 2 illustrates the system structure of the complete robot system, including a remote terminal. The task requires the robot to carry high payload during its walking on uneven terrain. Thus, the robot is designed to use legs based on a spatial parallel mechanism (UP-2UPS). Each leg has 3 degrees of freedom. The parallel mechanism makes the robot competent to carry a payload of 400kg, while the robot weighs about 270kg.

To make sure there is no electric device near the hazard environment which the foot-tip may experience, the servo motors that actuate the legs are installed on the upper side of the leg, which is also an advantage of the parallel mechanism. The hexapod robot has 18 servo motors in all. Each of them is a 400 Watts 3-phase BLDC (Brushless Direct Current) motor. The nominal torque of the motor is 0.747 Nm. Each servo motor has an independent drive that controls the motion. This demands for exchanging data between the controller and the drives at high bandwidth. Thus, the EtherCAT real-time industrial field bus is used to connect all the drives and the controller. The bandwidth of the bus is 100 Mbps. The real-time hardware is only fully-functional under the real-time software. Hence, the controller is an industrial PC running a Linux operation system with a patched real-time kernel. All the motion control algorithms, kinematics model and dynamics model are implemented and optimized in the real-time domain. All of these require a high-performance computer. Currently, the industrial PC has a 2249 MHz quad-core x86-64 CPU and 8 Gb memory. With this computer, the robot model can be computed in less than 0.3 ms. The control loop frequency is 1000 Hz. There is no force sensor or other sensor mounted on the foot-tip, which increases the risk of system failure. Home switches also have been removed to reduce the complicacy of the robot. The robot is connected to a remote computer wirelessly; the industrial PC can be accessed through a GUI program designed to communicate with the control program. For the robot, four 24V lithium-ion batteries serve as the power source of all electric parts.

Fig. 1 Robot Octopus III is a robot designed for carrying high payload when traversing uneven terrain. It has unique parallel mechanism legs

2.2 Mathematical Model

The mathematical model helps planning the motion of the robot and identifying the state of the robot. As mentioned before, kinematics model and indirect force estimation model are implemented in the real time robot control system. These models are established in unified coordinate frames attached to the robot, as shown in Fig. 3. There are three coordinate frames in the figure. C_w represents the world coordinate frame. The y-axis of the world coordinate frame is parallel to the gravity direction. C_r represents the robot coordinate frame. It is attached to the robot body. C_l^i represents the single leg coordinate frame attached to the i-th leg. As the robot has six legs with same structure and dimension, the single leg kinematics model is described.

2.2.1 Kinematics Model

The UP-2UPS mechanism of the leg is a spatial parallel kinematics mechanism. It has 3 degrees of freedom. The electric motor is connected to the ball screw through belt and gears. Thus, the three prismatic joints of a leg are the active joints. The direct kinematics model takes the length of the prismatic joint as the input. The output is the coordinates of the foot-tip (Eq. 1).

$$[E_x, E_y, E_z]^T = f(l_1, l_2, l_3) \tag{1}$$

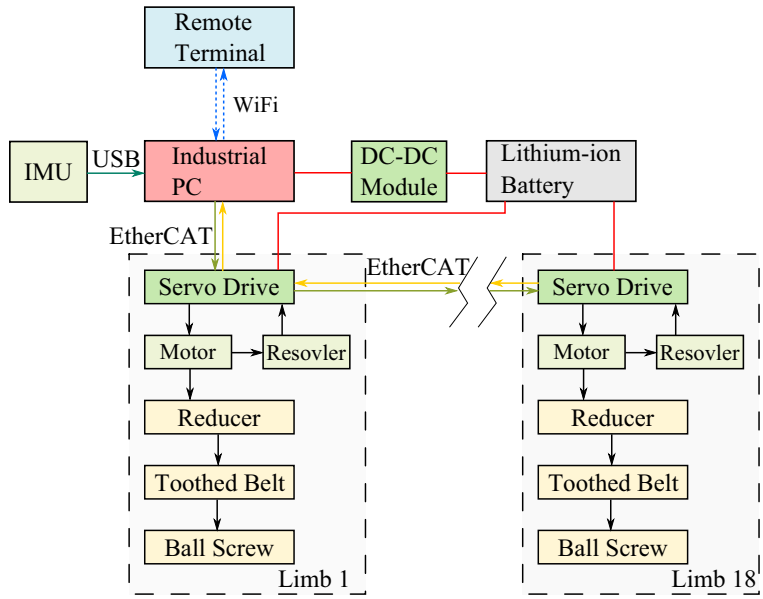

Fig. 2 The system structure of the robot Octopus III. There is no wire connected to the robot when it is running. Four lithium-ion batteries are the power source of all electric devices installed on the robot. The core of the control system is an industrial PC running real-time Linux. Each limb has one corresponding drive. The drive controls the motor of the limb. The motor thus controls the displacement of the prismatic joint of this limb through a reducer, a toothed belt, and a ball screw. All drives are connected through the EtherCAT real-time network

where

E_x, E_y, E_z– coordinates of the foot-tip,
l_{p1}, l_{p2}, l_{p3}– length of the prismatic joints.

Observing the mechanism's UP limb, it can be found that the relation between two different positions of a same point on the foot can be described by three transform matrices, see Eq. 2. Two rotation matrices are produced by the universal joint. One transition matrix is the result of the prismatic joint. The three lengths, l_{p1}, l_{p2} and l_{p3} can be used to calculate the two rotation matrices. The transition matrix can be easily calculated from l_{p1}. Thus, after some calibration on the real robot, the direct kinematics model is established.

$$[E_x, E_y, E_z]^T = \mathbf{M^1_{rot}} \cdot \mathbf{M^2_{rot}} \cdot \mathbf{M_{tran}} \cdot [E^0_x, E^0_y, E^0_z]^T \quad (2)$$

The inverse kinematics model takes foot-tip position as the input. The output consists of the displacements of the three prismatic joints. Again, the derivation starts from the UP limb. With the coordinates of the foot-tip, two rotation angles of the universal joint of the UP limb are calculated. The displacement of the prismatic joint of the UP limb can also be computed. Thus the transform matrix can be derived. By the transformation matrix, the displacements of the two prismatic joints in UPS limbs can be computed. Finally, the inverse kinematics model is established.

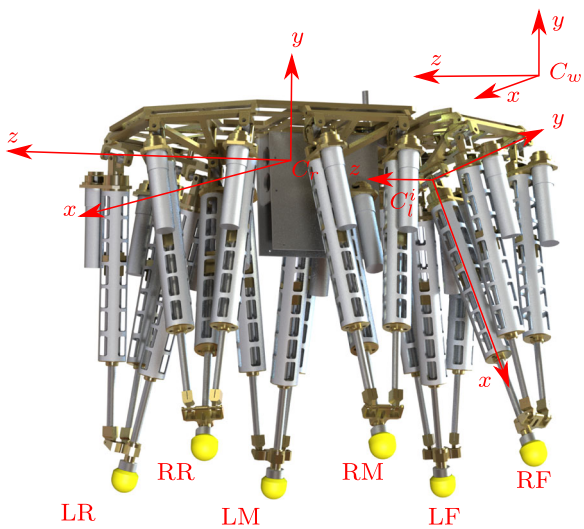

Fig. 3 Coordinates frames of the robot model. In the robot body coordinate frame C_r, the sagittal plane is the yz-plane; the xy-plane is the frontal plane; the zx-plane is the transverse plane. The legs are label as LF(*Left Front*), LM(*Left Middle*), LR(*Left Rear*), RF(*Right Front*), RM(*Right Middle*), and RR(*Right Rear*)

2.2.2 Indirect Force Estimation Model

Based on this robot, an indirect force estimation model is developed [17]. As illustrated in Fig. 4, the external force n is applied to the foot tip. To balance this force, forces f_1, f_2 and f_3 will generated on the prismatic joints.

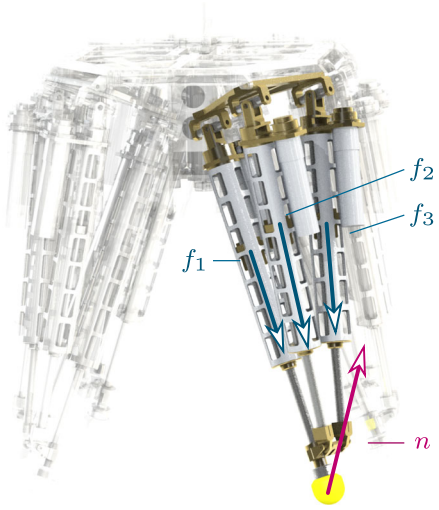

Fig. 4 Indirect force estimation. The three motors torque data are used to estimate the external force exerted on the foot. It is a linear transformation $M : \vec{n} \rightarrow \vec{f}, \vec{n} \in R^3, \vec{f} \in R^3$

These three forces can be estimated from the motor current. The indirect force estimation model uses the force Jacobian matrix of the leg mechanism is used to map these three force to the external force. The force Jacobian can be derived after the kinematics model is established.

$$[n_x, n_y, n_z]^T = \mathbf{M_{Jac}} \cdot [f_1, f_2, f_3]^T \tag{3}$$

Thus, the six legs of the robot become six three-axis force sensors. Then the robot can detect obstacles and ground. The proposed gait is also based on these implementations.

3 Human Experiment

3.1 Human Blind Walking

For a normal human being, the locomotion involves three systems, which are the visual system, the vestibular system, and the somatosensory system [22]. The visual system plays a crucial part in human life. We do most activities at daytime and switch on the light at night so we can see. During the walking, we look ahead to regulate our foot trajectories before we step on somewhere [23, 24]. The vestibular system consists of the balance organs in the inner ear [25]. The system senses rotational movements and linear accelerations. Research reveals that vestibular system may be functional when leg muscles control the balance [26]. The somatosensory system provides the central nerve system the image of our body. It takes both exteroceptive inputs and proprioceptive inputs [27]. During the walking process, the somatosensory system provides feedback about the contacts, joint angle, muscle tension, etc.

Components with similar functions can be found on the robot Octopus III (Fig. 5) – a vision module uses a Kinect [28]; a "vestibular system" is realized by an IMU; a partly-implementation of a "somatosensory system" is archived by resolvers and the indirect force-estimation model. Table 1 compares the involved sensory systems in the normal walking and the blind walking of the human and the robot. To obtain some ideas that shed light on the robot gait design, an experiment is designed and performed to observe how human walks without vision.

3.1.1 Experiment Settings

Figure 6 shows the snapshots taken from the video footages of two experiments (one on the uneven terrain and one on the flat ground). For the uneven

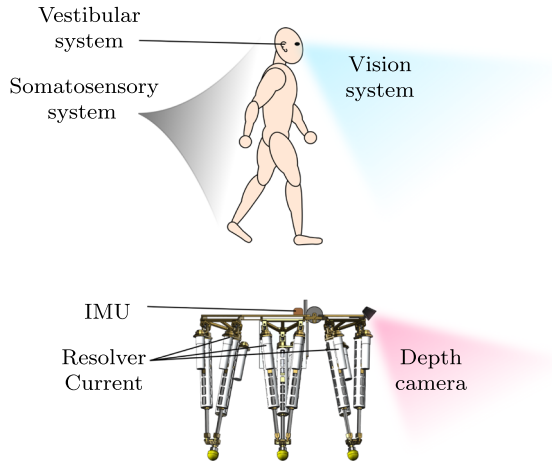

Fig. 5 Human walking involves three systems, the vestibular system, the vision system and the somatosensory system. The robot walking involves devices with similar functions. The depth camera measures the distance just like the binocular vision system of a human. The IMU measures the gravity orientation, angular movement and attitude, which is similar to the vestibular system. Resolvers and motor currents provide the position and force information of the moving limb, which is the role played by the somatosensory system in a human body

Table 1 Involved sensory systems in the normal walking and blind walking of the human and the robot

	Normal walking		Blind walking	
	Human	Robot	Human	Robot
Path	Vision system	Computer vision	Not available	Not available
Balance	Vision system	IMU	Vestibular system	IMU
	Vestibular system		Somatosensory system	
	Somatosensory system			
Proprioception	Somatosensory system	Resolver	Somatosensory system	Resolver
		Current		Current

In the nighttime or a dim environment, the computer vision system may not as effective as in an illuminated environment. Thus, in this paper, the robot Octopus III is regarded as a robot without any vision system. As a result, the robot walks in such a condition that it uses its legs more like a human without vision. The comparison shows the similarity between human blind walking and robot "blind" walking. It is reasonable to investigate human blind walking when we are trying to design a gait for the robot without the vision

situation, the obstacles were constructed by a pile of bricks. Each brick was about 0.1m in height, 0.3m in width and 0.6m in length. Along with the walking direction, there was a thin string hanging over the obstacles. This string was there to make sure volunteers keep walking in the right direction. Meanwhile, it did not provide any other support to volunteers. In the experiment, the volunteer was required to walk from the right side of the obstacles to the left side. The volunteer wore an eye mask from the beginning to the end. Thus, there was no vision during the walking. First attempts of the experiments revealed that any glance at the obstacles would help the volunteer planning the locomotion. The final experiment procedure required the volunteer to wear the eye mask from the very beginning to the end. In this way, the volunteer had no prior knowledge about the obstacle. There was also a small light ball attached to foot as an indication of the foot-tip position. This was for the convenience of tracking the trajectory of the foot-tip.

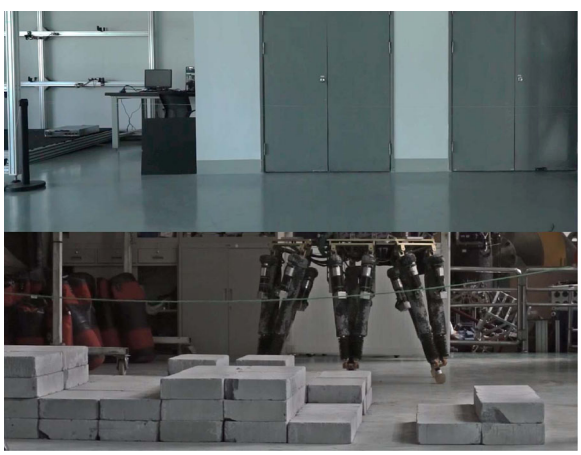

Fig. 6 Experiment settings. Two ground conditions are used to observe human blind walking. A flat ground and some obstacles constructed by piles of bricks were used in the experiments. Comparing human blind walking on the flat ground and the uneven ground helps us understanding human behavior on the uneven ground

3.1.2 Experiment Results

In all, thirteen experiments have been performed with five healthy volunteers. Each of them was told about the experiment process before the experiment and signed an informed consent form. The study protocol was approved by the local Ethics Committee of Shanghai Jiao Tong University. Each time the obstacles were different. The rest figures in this section are captured on the video footages from the experiments. These video footages have been processed by digital image processing technology, and the foot-tip trajectories are added to each frame of the video. Figure 7 illustrates the trajectories gathered from the experiments.

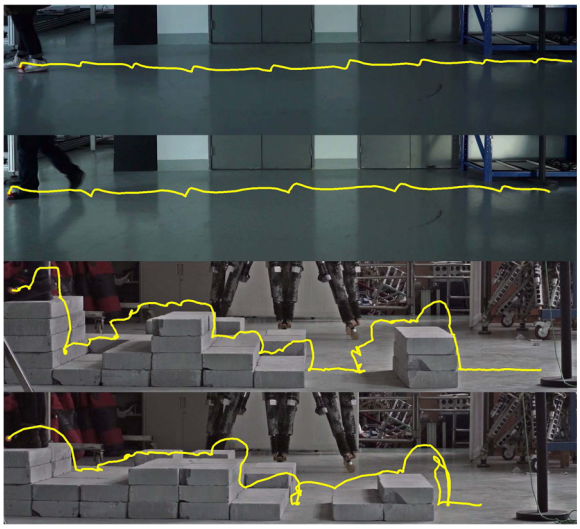

Fig. 7 Foot-tip trajectories gathered in the experiments. The above two trajectories were collected during blind walking on the flat ground. The bottom two were obtained on uneven ground. The trajectories from the flat ground are more like a recurrence of the same pattern

Figure 8 compares the walking properties in the two walking conditions. Figures 9, 10, 11, and 12 describe the trajectories in details.

Figure 11 shows the trajectories during the volunteers stepping on the obstacles. It's obvious that the volunteer raised his foot higher than before. But what interests us are the trajectories highlighted by the red boxes. After the first contact with the obstacle top, the volunteer did not stop and switch the swing foot immediately. The volunteer used the swing foot to make another small motion, which could help the volunteer to gather more information about the surroundings near the first ground contact point. After this motion, the volunteer placed the foot to a "safer" position. For example, at first, the volunteer placed the foot right on the edge of the obstacle. Then he or she moved the foot-tip around that point. Finally, the volunteer placed the foot-tip away from the edge. So the volunteer would not fall because of the ditch in front of him. This small motion caught the eye of us because normally, with the help of the vision, people do not walk in this way. We believed that this phenomenon reveals the way human deal with walking without vision on the uneven ground.

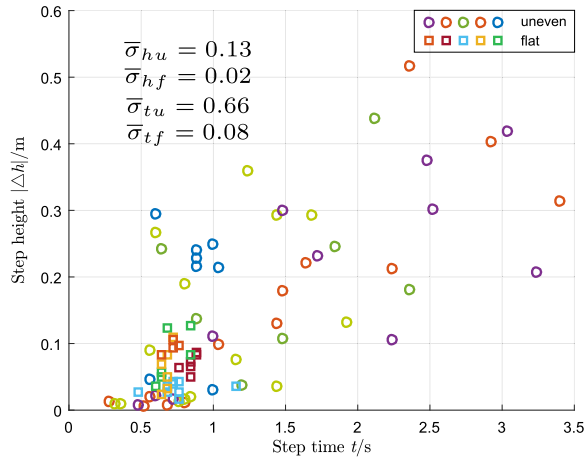

(a) Step height and step time.

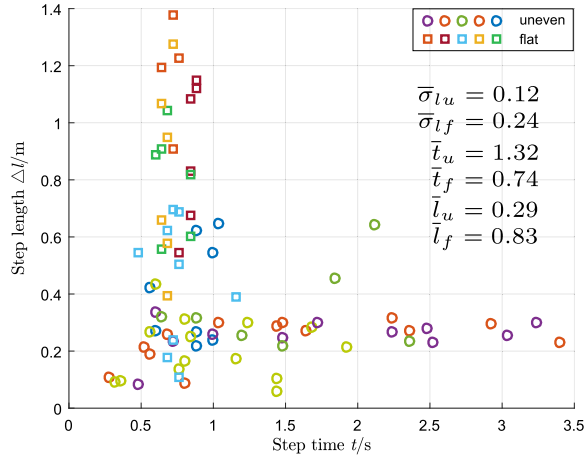

(b) Step length and step time.

Fig. 8 The round markers represent the data gathered on the uneven ground. The square markers represent the data gathered on the flat ground. The different colors differentiate between different samples. Figure 8a compares the step height and the step time. The average of the sample standard deviations of the step height ($\overline{\sigma}_{hu} = 0.13$) and step time ($\overline{\sigma}_{tu} = 0.66$) from the uneven ground were bigger than those from the flat ground($\overline{\sigma}_{hf} = 0.02$, $\overline{\sigma}_{tf} = 0.08$). These imply that both the step height and the step time varied more on the uneven ground. Figure 8b compares the step length and the step time. The step length of flat walking varied more than walking on uneven ground (The average of the sample standard deviations of the step length on the flat ground was $\overline{\sigma}_{lf} = 0.24$, and on the uneven ground $\overline{\sigma}_{lu} = 0.12$.). While walking on the uneven ground, the step length (Average length $\overline{l}_u = 0.29m$) was shorter than walking on the flat ground(Average length $\overline{l}_f = 0.83m$). Meanwhile, the average step time on the uneven ground was longer($\overline{t}_u = 1.32s, \overline{t}_f = 0.74s$)

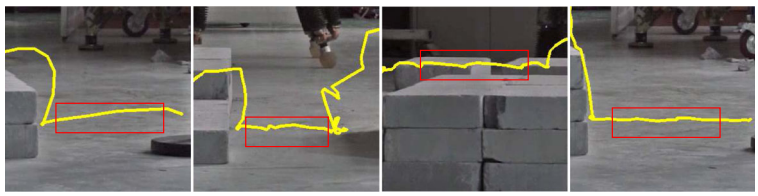

Fig. 9 Foot-tip trajectories on the flat sections. The red boxes mark sections of interest. At first, the step height is rather low. The volunteers were not likely to use larger step height before any contact with an object. However, if the previous situation has convinced the volunteer that there would be an obstacle ahead, then the volunteer will raise the leg more than ordinary

4 Gait

In the previous section, experiments on human have been discussed. Based on the observation and analysis of these experiments, a set of rules are designed to generate adaptive gait for the robot Octopus III. With this gait, the robot can traverse through certain uneven terrain.

4.1 Inspired by Human Blind Walking Experiments

In the human blind walking experiment, it can be concluded that static gait is applied to get better stability on uncertain terrain. Thus, for the six-legged, a static tripod gait is chosen as the basic gait for its stability. Using this gait, the robot can easily put its center of gravity into the support polygon. Then variations are added to the basic gait to increase its flexibility to adjust the trajectory during the walking on the uneven terrain.

Figure 13 illustrates different single foot trajectories. When there is no feedback from the foot-tip, rectangle gait could be more robust than semi-ellipse gait on rough terrain. However, the semi-ellipse gait has a smoother velocity curve than the rectangle gait. Here, the semi-ellipse gait is chosen for its better velocity property. Then, with the help of the foot-tip force feedback provided by the indirect force-estimation model, the semi-ellipse gait becomes more adaptive, as described in the following paragraphs.

Figure 14a describes the gait designed for overcoming obstacles. Subfigure (1) and subfigure (2) illustrates how the gait trajectory changes when the foot collides an obstacle. The robot will move back its leg when the steep increase of external force occurs. After the foot is withdrew, the robot will raise its foot, trying to step on the obstacle. Subfigure (2) illustrates that the robot will try more than once to step on the obstacle. It is clear that the robot could not raise its foot unlimitedly, a fuse protection mechanism will be discussed later. Subfigure (3) illustrates when the robot foot is on the obstacle, it will move like on the ground; the trajectory is almost the same except there exists an offset about the body coordinate frame. Subfigure (4) illustrates how the robot steps down from the obstacle. The robot uses the indirect force-estimation model to detect if the foot-tip has contacted the ground. Also, the supporting force provided by the ground is calculated.

In the human blind walking experiment, it is observed that the volunteers used some small motions to detect the structure of the terrain near the foot. This mechanism has been added to the basic gait. Figure 14b illustrates how this small motion functions

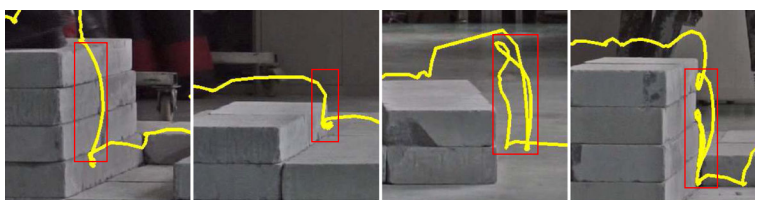

Fig. 10 Foot-tip trajectories during touching the obstacle. After contacting with an obstacle, the volunteer adjusted the step height once or more times to step on the obstacle. In this process, some volunteers moved back their feet a little and increased the step height, and some volunteers moved their feet along the obstacle surface to find out the size of the obstacle then stepped on the obstacle. To be clear, in these experiments, all the obstacles were limited at a suitable height for volunteers to step on

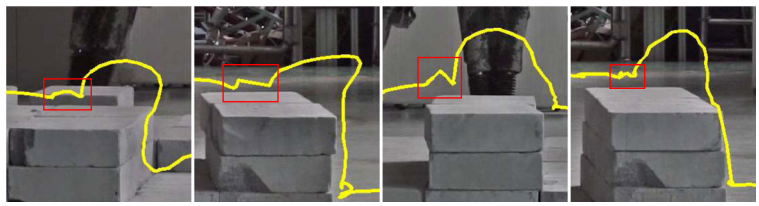

Fig. 11 Foot-tip trajectories during stepping on the obstacle. After the volunteer had stepped on the obstacle, a tentative movement (trajectories marked with the *red boxes*) of the foot helped the volunteer to step on the safer place, where was not too close to the edge

during the robot walking. As mentioned before, the trajectory starts from the left side of the figure. In subfigure (1), the simplest situation is illustrated, where the terrain is flat. The blue trajectory is the basic gait, and the yellow trajectory is employed to do the detection. In this situation, after the green trajectory, the foot will finally stop in the middle of the two ground contact points. In subfigure (2), there is an obstacle. After raising the height, the leg steps on it. However, the first contact point is very close to the edge. With the small motion, the foot's final position is away from the edge, which prevents the foot from slipping off the edge. On the other hand, there is a possibility that the foot is at first stopped just a little behind an edge. In this situation, the detection trajectory will find there is a ditch in front of it. Then the end point of the green trajectory is behind the end point of the blue trajectory. This is also a mechanism to avoid the foot slipping off the edge. Subfigure (4) illustrates how the foot steps down from the edge with small motion trajectories.

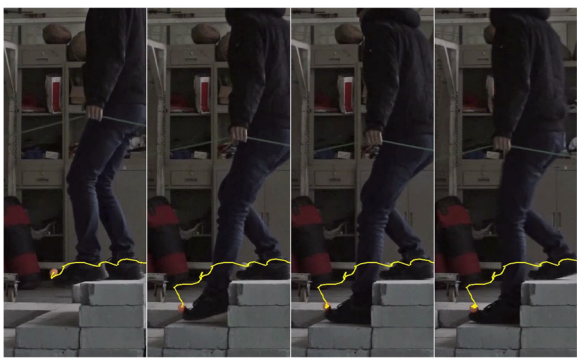

Fig. 12 Foot-tip trajectories during stepping down the obstacle. The step length was short during walking on uneven ground. It is worth noticing that the center of the body did not move out of the supporting foot until the swing foot had actually stepped on the stable ground, which implies that the volunteer was using a static gait while there was no vision system to help him to plan the next step

In human experiments, when the volunteer found there is an obstacle ahead, he or she would adjust the foot height of next step. Figure 14c illustrates a situation that small motion detects an obstacle. In this condition, the robot has the perception that there is an obstacle ahead. So in the next gait, the robot will raise its foot higher than before directly, trying stepping on the obstacle.

Figure 14d illustrates the fuse protection mechanism of the proposed gait. Two situations are described in the figure. If the obstacle is too high (if an obstacle is too high to climb, then it is referred as a wall.) or the ditch is too deep then the robot will stop its motion, avoiding the useless attempts.

4.2 Adaptive Gait for Robot Octopus III

Figure 15 illustrates the transitions of gait trajectories by the proposed rules. The blue box represents the leg supporting the body. The blue circle represents the leg swinging. A wall or a deep ditch stops the robot. Otherwise, the leg motion is a loop of swinging and supporting. And during this process, the proposed gait has variations to overcome obstacles, giving the robot capability to walking through uneven terrain.

For each foot in each step, the swing trajectory is a sequence of curves. These curves could be arcs of ellipses or straight lines. Because the real-time control cycle is 1ms, the generating method of the trajectory

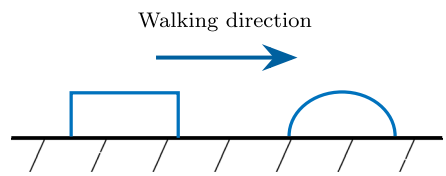

Fig. 13 Different gait trajectories. The trajectory is composed of one or more curves. The leg trajectory is a half ellipse as no sudden change in position and velocity is expected unless the foot contacted with the environment

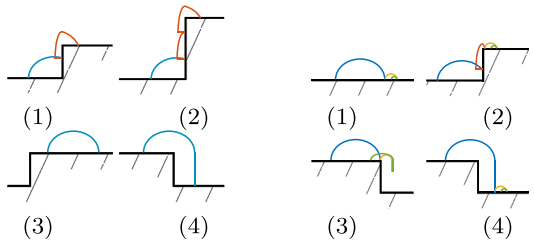

(a) Reaction of the obstacle.

(b) Reaction of the obstacle.

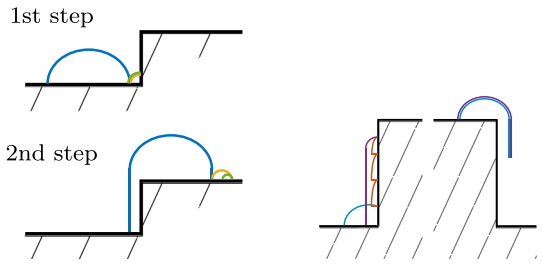

(c) Prediction about next gait.

(d) Reactions to the limits

Fig. 14 Gait patterns inspired by human blind walking behaviors. Figure 14a illustrates that the robot will adjust its trajectory when the foot contacts with an obstacle. The foot will move back immediately after contacted with the obstacle. The direction is determined by the force direction from the indirect force-estimation. Figure 14b is based on Figure 14a. The tentative motion is added to avoid standing too close to the edge. Figure 14c illustrates another use of the tentative motion. It helps to determine the height of the next step. Figure 14d illustrates the behavior when the obstacle reaches the limit of the leg workspace; the robot will stop trying to walk through the obstacle

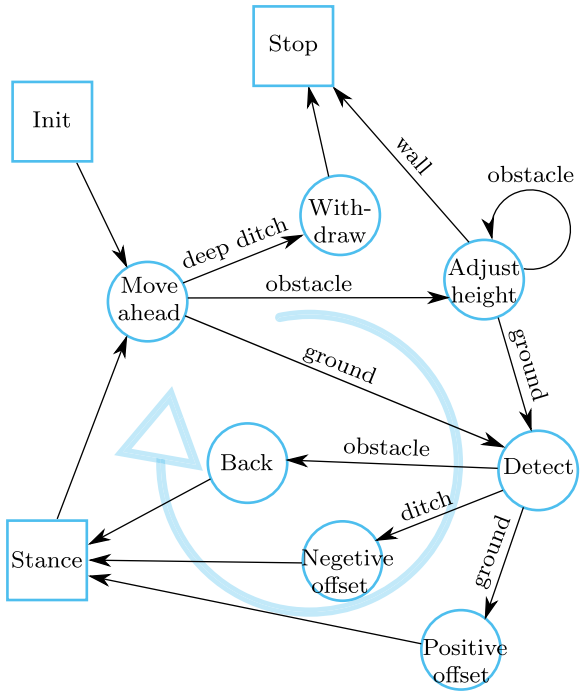

Fig. 15 Gait trajectory transitions. Each blue circle represents a curve in the swing state of the leg, while blue box represents the support state of the leg. The trajectory of each foot is controlled by a finite state machine. The trajectory consists of a group of curves. These curves must be continuous in position. The velocity may experience a change when the foot-tip contacts with the ground or the obstacle. The loop in these transitions represents the way robot walks. In all, six loops are formed in this transitions. The variations give the robot ability to negotiate with the environment

cannot be complicated. Thus, the algorithm uses a trivial way to regulate the trajectory. Firstly, the length of the trajectory is calculated. For the ellipse arc, a numerical method is used to evaluate the length unless the curve is a semi-ellipse or a quarter-ellipse. In these situations, the arc length can be derived from the circumference of the ellipse, which can be computed by Ramanujan's approximation formula (Eq. 4).

$$\begin{aligned} S_{ell} &= \pi(a+b)(1+\frac{3h^2}{10+\sqrt{4-3h^2}}) \\ h &= \frac{a-b}{a+b} \end{aligned} \tag{4}$$

After obtaining the trajectory length S, a trapezoidal velocity profile is used to calculate the duration of the swing (Denoted as t_{swing}). For a given max velocity v_m, acceleration a_a, and deceleration a_d, t_{swing} is calculated by Eq. 5.

$$\begin{aligned} S &= \sum S_i \\ t_{swing} &= \sqrt{\frac{2S(a_a+a_d)}{a_a a_d}},\ S \le \frac{{v_m}^2(a_a+a_d)}{2a_a a_d} \\ t_{swing} &= \frac{S}{v_m} + \frac{v_m(a_a+a_d)}{2a_a a_d},\ S > \frac{{v_m}^2(a_a+a_d)}{2a_a a_d} \end{aligned} \tag{5}$$

During the walking process, the trajectory is generated as $T(t), t \in [0, t_{swing}]$. As a group of curves, the trajectory is a piecewise smooth function of time. The trajectory has C^0 continuity. The discontinuity in speed occurs when the foot collides with the ground or the obstacle. After these events, the trajectory generator regenerates a new trajectory based on the current

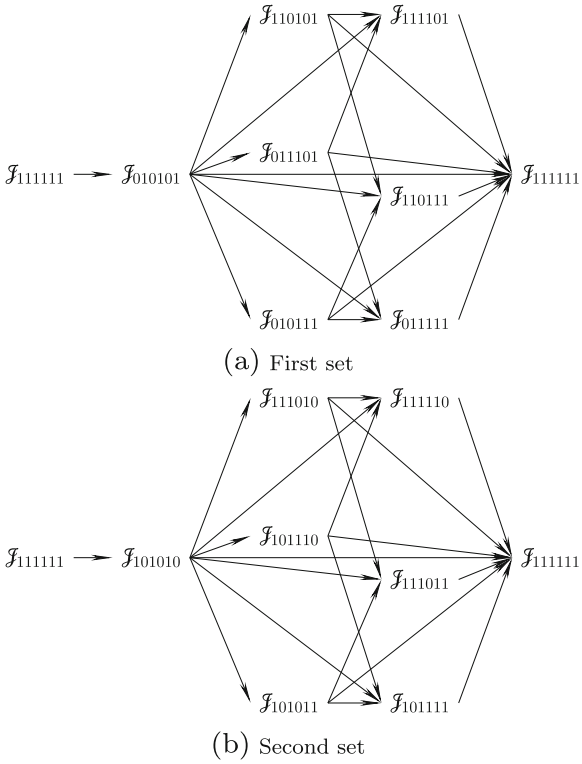

Fig. 16 The ground contact transitions of each leg set. The proposed alternating tripod gait divides the legs into two sets. These sets swing and stand alternatively. The first set consists of leg LF, RM and LR (Subfigure (**a**)). The rest legs form another group (Subfigure (**b**)). Here, the contact means that the leg begins to support the body weight

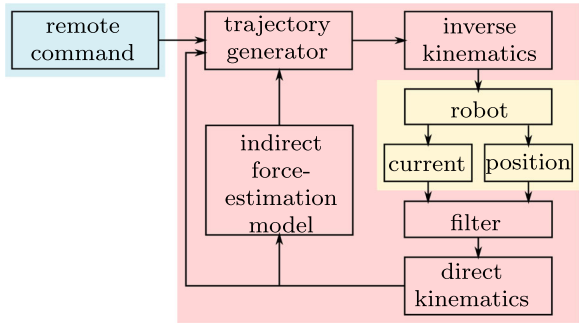

Fig. 17 Robot control process. The gait transitions described in Fig. 16 are implemented in the trajectory generator. The foot trajectories are generated in the Cartesian coordinate system. Thus these points are mapped to the joint space by the inverse kinematics model. Then the joint space data are sent to the drives on the robot. On the other hand, the feedback joint space data are mapped to the Cartesian coordinate system by the direct kinematics model

foot position and contact condition. For the trajectory $T(t)$, a mapping $q(t)$ is introduced to mapping $[0, t_{swing}]$ to I (Unit interval [0,1]) as described in Eq. 6. Thus, the same trajectory can be expressed as $\mathcal{S}(q), q \in I$. For each single curve $\mathcal{S}_i$ in the trajectory, the parameter also runs over I (Eq. 7).

$$\begin{aligned} &T(t) = \mathcal{S}(q(t)) \\ &t \in [0, t_{swing}], q(t) \in [0, 1] \end{aligned} \tag{6}$$

$$\begin{aligned} &\mathcal{S}(q) = \mathcal{S}_i(\tfrac{q-q_{i-1}}{q_i-q_{i-1}}) \\ &q_{i-1} \le q < q_i, i = 1 \ldots n, q_0 = 0, q_i \le 1 \end{aligned} \tag{7}$$

Johnson and Koditschek proposed the ground reaction complex [29] to describe the possible ground contact transitions of a legged robot. In our research, the robot has six legs arranged in an axial-symmetric way. Thus, we have an index set $\mathcal{J} := \{F, M, R\} \times \{L, R\}$, where F, M, R represent "front", "middle" and "rear". L, R represent "left" and "right". For $\mathcal{J}$, the subscript j is a binary sequence sorted by (LF, LM, LR, RF, RM, RR) corresponding to each foot of the robot. Thus, $\mathcal{J}$ means leg LM, RF and RR contact with the ground. Figure 16 illustrates the possible transitions of ground reaction conditions of the proposed gait.

The algorithm is implemented in the real time control program. Figure 17 describes the structure of the control system software used in the experiment.

Fig. 18 Experiment settings. The uneven ground is constructed with two layers of the bricks, which is not as high as the obstacle in the human blind walking experiment. This is because the workspace of the leg mechanism is smaller than the serial limb of the human. The max displacement of the prismatic joint is 0.3m, while the height of the brick pile is 0.2m. Moreover, the pile of bricks is placed on the right side of the walking direction, which makes the obstacle not symmetric about the sagittal plane

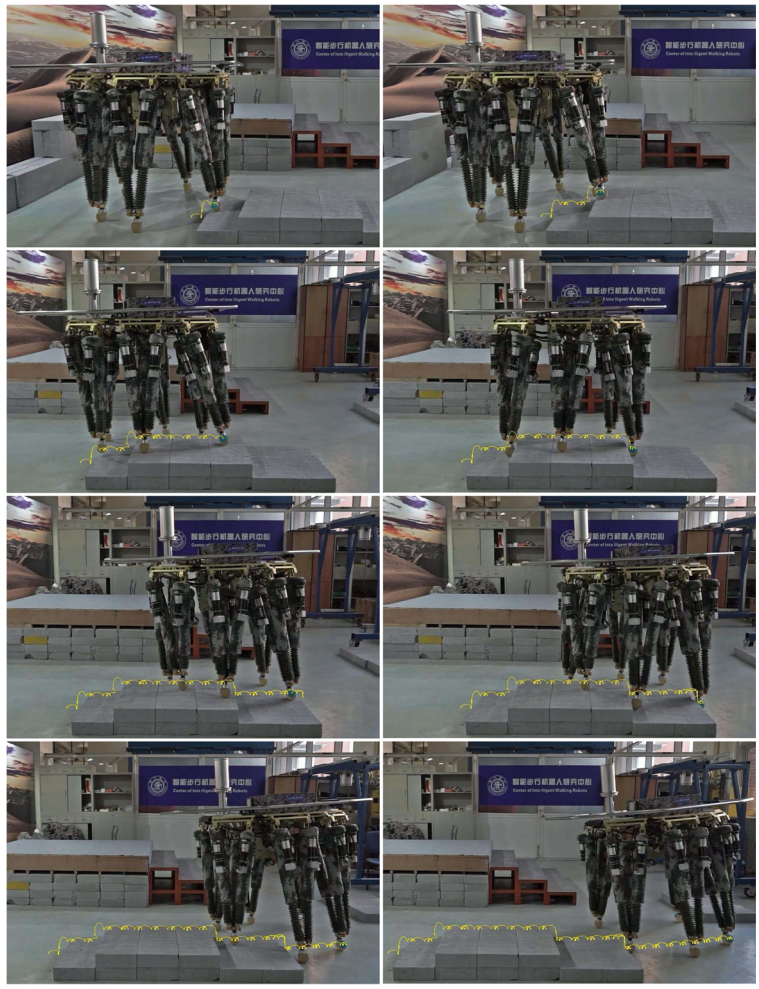

Fig. 19 Snapshots from the experiment video. The Robot walked through the uneven ground using the proposed alternating tripod gait. The RF foot was attached with a blue mark. By tracing the blue mark, the trajectory was plotted as the yellow curve

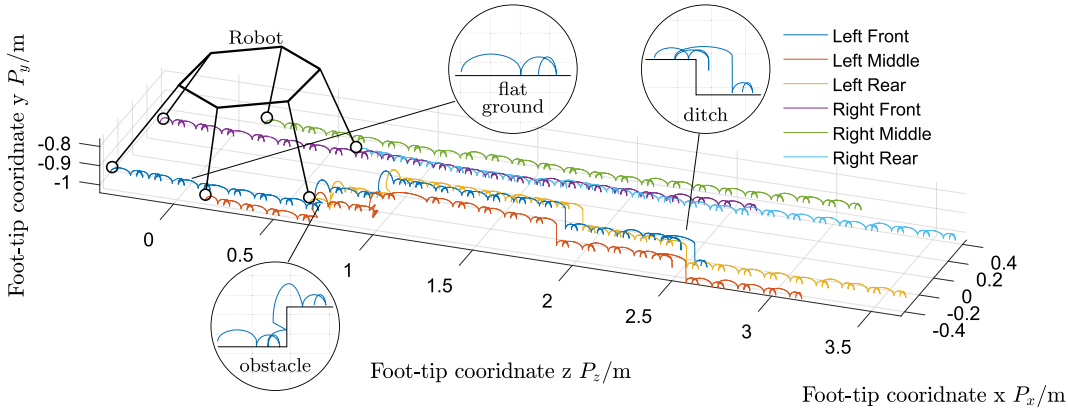

Fig. 20 Trajectories of robot legs in the world coordinate frame C_w. Curve with ifferent color represents different leg of the robot. The robot control program will record the data uploaded by the drives. This figure shows the position data gathered during the experiment, although the trajectory of each step was planned under body coordinate frame (See Fig. 3) during the walking. The above trajectories are plotted in the world coordinate frame of the robot coordinate system. Obviously, on the right side of the walking direction, the ground contact points of the three legs envelop the obstacle. On the other side, the ground is much more flat

5 Experiment on the Robot

This section describes the experiments on the robot. Results of the experiments are also plotted and analyzed.

5.1 Experiment Settings

In the first experiment, an uneven ground was constructed from a pile of bricks. Figure 18 is a photo of the experimental environment. The robot walked through these bricks during the experiment using the proposed method. After that, the proposed gait was also tried on different obstacles, including a slope, sandbags, etc.

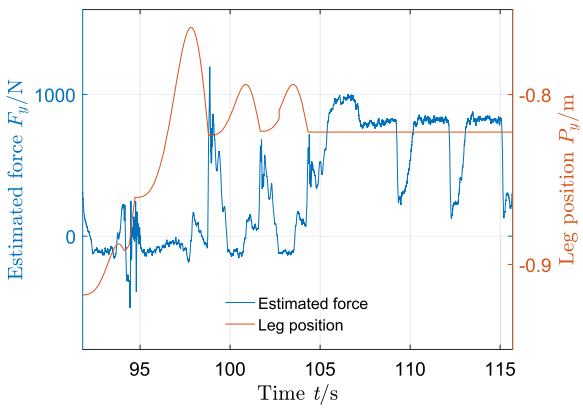

(a) Estimated external forces along y-axis in one cycle.

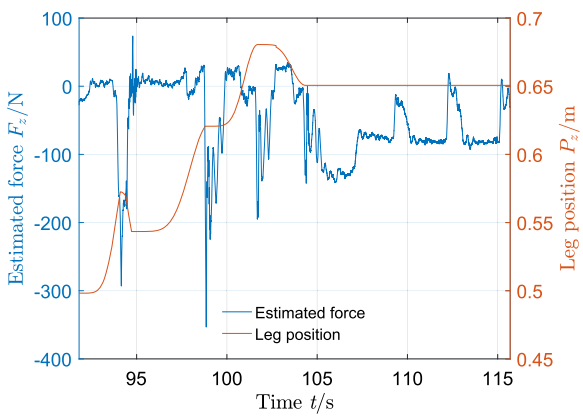

(b) Estimated external forces along z-axis in one cycle.

Fig. 21 Positions and estimated forces of the LR(*left rear*) leg in one cycle. The P_y curve shows that the foot stepped on an obstacle during this cycle. Before 95th second, the leg experienced a sudden change in the estimated force along y-axis(F_y). This is because the 3 degrees of freedom of the leg are coupled with each other. If we look at Fig. 21b, there was a much larger force change before 95th second. This indicates the robot foot has contacted with an obstacle in the walking direction. Thus the leg moved back a little and adjusted its height as shown in the above figure. After 105th second, the leg was in supporting state. Although the estimated force changed several times, which were caused by the motion of the other legs, the leg stayed at the same position

5.2 Experiment Results

Figure 19 provides a set of snapshots from the video footage of the experiment.

One leg was traced by the computer vision program. Its trajectory is illustrated in the pictures. The robot gradually stepped on the obstacles, then walked on the obstacle, and finally, walked through it. Figure 20 illustrates the trajectories of all legs during the experiment. The data were returned by the resolvers installed on the robot. Legs on the left side walked through the obstacles one by one, while legs

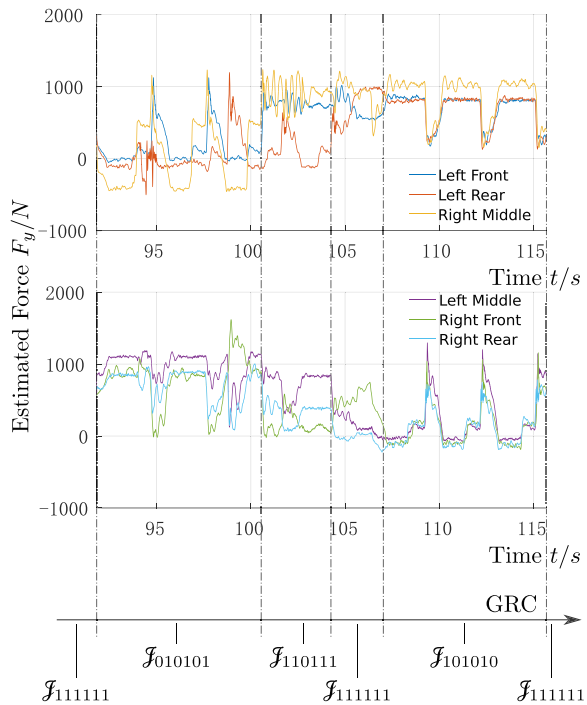

Fig. 22 External forces along y-axis of all legs in one cycle. These data are the result of the indirect force-estimation. The difference between the swing state and the stance state is obvious. Leg LF, LR, and RM moved at first, then leg LM, RF, and RR. The force along y-axis was the supporting force. In this cycle, the ground contact transition is $\mathcal{J}_{111111} \rightarrow \mathcal{J}_{010101} \rightarrow \mathcal{J}_{110111} \rightarrow \mathcal{J}_{111111} \rightarrow \mathcal{J}_{101010} \rightarrow \mathcal{J}_{111111}$, which is one of the routines plotted in Fig. 16

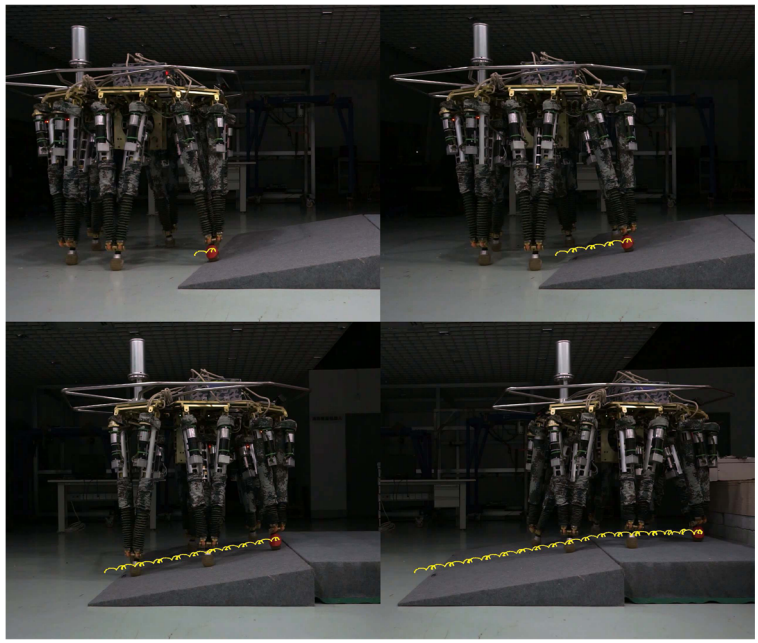

Fig. 23 The robot walked on a slope. The slope is made of boards and covered with a carpet. The slope is about 10°. The robot climbed on this slope during the experiment. Since there was an angle between the slope and robot walking direction on the sagittal plane, each step length was shorter on the slope. In the experiment, the robot recognized the slope as an obstacle occasionally. However, for climbing the slope, this behavior made no big difference

on the right side walked on the flat ground. In each step, the robot tried different locations before actually stepping on a certain location.

Figure 21 illustrates the force and position of leg LR curves during a cycle of the experiments. Figure 21a illustrates how estimated external forces and positions of leg LR varies along the y-axis in the experiment. From 96th second to 105th second, the foot-tip contacted with the ground for three times. Then, the leg stopped moving and supported the weight of the robot. From 105th second to 115th second, the leg was supporting the body weight. However, when other legs contacted with the ground, the weight on the rest legs became smaller.

Figure 21b illustrates how estimated external forces and positions varies along the z-axis. At about the 94th second, the foot collided with an obstacle. Then it came the reflex reaction. However, from 96th second to 105th second, there was also a big force along z-axis. But this time the robot contacted with the ground, so there was no withdraw reaction here.

Figure 22 illustrates the forces on the y-axis direction of one cycle. Leg LF, LR, and RM started to move at first, then the body, and finally leg LM, RF and RR. The three peaks show the three contacts when robot found the right location for the feet.

The proposed gait is designed to be adaptive, it was tested in various terrains. Beside the bricks pile, we

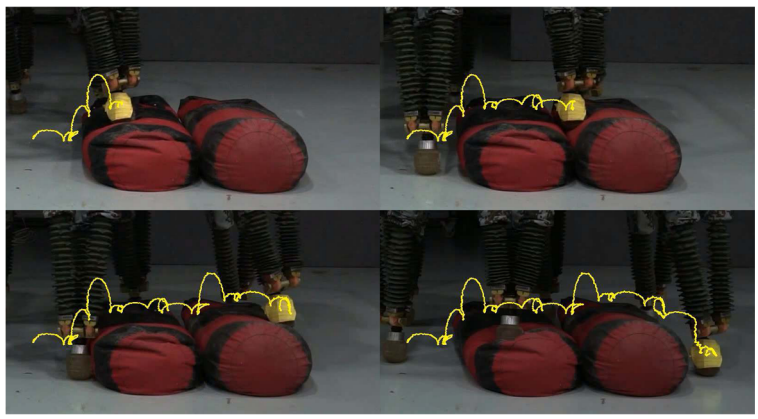

Fig. 24 The robot walked through sandbags. The sandbags were soft, and their shapes were irregular. But the robot was managed to overcome them by the proposed gait. Although the gait is designed based on square bricks, this experiment demonstrated its robustness

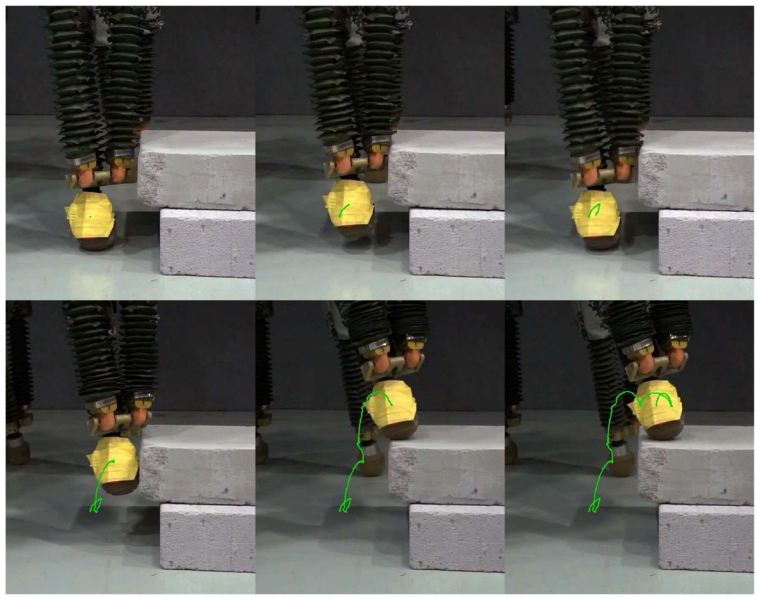

Fig. 25 Robot stepped on an obstacle using indirect force-estimation. These snaps illustrate that indirect force-estimation has a large sensing area. Although the upper-side of the ankle contacted with the obstacle at first, the robot still detected the obstacle effectively. If the robot used a force sensor installed on the foot-tip, it could not be able to detect this obstacle

also let the robot walk through a slope made of boards. Figure 23 shows the snapshots of the experiment video. The robot climbed the slope and maintained the body attitude.

Also, the obstacle with irregular shape was tested. Figure 24 shows the process of one leg of the robot overcoming two sandbags laying on the ground. As the obstacle shape varied, the gait trajectories also changed to track it.

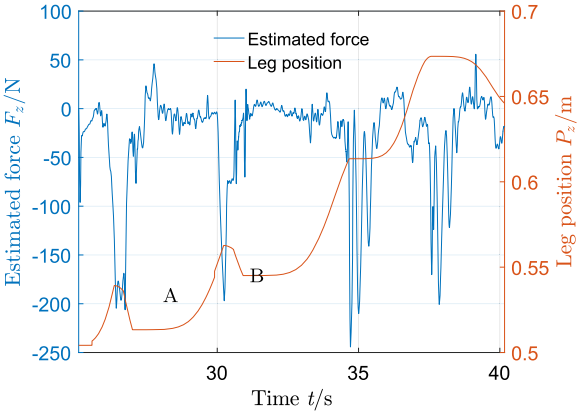

Fig. 26 The position of the foot-tip (P_z) and the external force (F_z) along the z-axis. This figure is corresponding to Fig. 25. The walking direction was the positive direction of z-axis. At point A, the upper-side of the ankle contacted with the obstacle. At point B, the foot-tip contacted with the obstacle. The indirect force-estimation was effective in both situations

Another kind of obstacle was also included in experiments. As shown in Fig. 25, the lower part of the obstacle was recessed. In this situation, the foot-tip can hardly contact the obstacle because the ankle or the leg would collide with the obstacle at first. Then if there was a force sensor installed on the foot-tip, it would be useless. However, the indirect force-estimation method can detect the obstacle. With the proposed gait, the robot leg climbed the obstacle after adjusting the foot height twice (Fig. 26).

6 Conclusion

In this paper, an adaptive gait for six-legged robot is proposed based on the observation of human blind walking. The human volunteers walked through even or uneven terrain when their eyes are covered, which were recorded by a camera. Through computer vision techniques, trajectories were extracted and analyzed to find out patterns in the human blind walking. Then, the adaptive gait is designed based on these patterns. The research of this paper is based on a six-legged walking robot without vision sensor. The robot has a spatial parallel leg mechanism (UP-2UPS). The indirect force-estimation method is implemented on the robot, which avoids the fragile force sensors. All the kinematics model and indirect force-estimation model has been implemented in the real-time operation system on the robot.

The proposed gait was tested on different types of ground. The robot walked through a pile of bricks with maximum height of 20cm. The step length was shorter on the slope because of the slope angle, while the robot walked on a 10° slope. The gait was not only tested on hard ground but also tested on soft materials. The experiment on the sandbags demonstrated the gait was of certain robustness on the soft ground. Also, the gait worked on the irregular shaped obstacles although it was designed based on the human walking experiments on the obstacle environment consisting of bricks. Another experiment demonstrated the proposed gait and indirect force-estimation had a larger sensing area than the force sensor installed on the foot-tip. When the obstacle contacted with the lower part of the leg rather than the foot-tip, the proposed method still could detect the obstacle and overcome it.

Acknowledgments The authors express sincere thanks to the editors, reviewers and all the members of our research group for their beneficial comments. The research work is supported by National Basic Research Program of China (973 Program) (No. 2013CB035501).

References

1. Vukobratović, M., Borovac, B.: Zero-moment point—thirty five years of its life. Int. J. Humanoid Rob. **1**(01), 157–173 (2004)
2. Park, J.H.: Fuzzy-logic zero-moment-point trajectory generation for reduced trunk motions of biped robots. Fuzzy Sets Syst. **134**(1), 189–203 (2003)
3. Kalakrishnan, M., Buchli, J., Pastor, P., Mistry, M., Schaal, S.: Learning, planning, and control for quadruped locomotion over challenging terrain. Int. J. Robot. Res. **30**(2), 236–258 (2011)
4. Ali, A., Moosavian, S., Dabiri, A.: Dynamics and Planning for Stable Motion of a Hexapod Robot. Advanced Intelligent Mechatronics (AIM), 2010 IEEE/ASME International Conference On, Pages 818–823. IEEE (2010)
5. Asif, U.: Improving the navigability of a hexapod robot using a fault-tolerant adaptive gait. Int. J. Adv. Robot. Syst. **9**(33), 2012–2024 (2012)
6. Ijspeert, A.J.: Central pattern generators for locomotion control in animals and robots: a review. Neural Netw. **21**(4), 642–653 (2008)
7. Liu, G.L., Habib, M.K., Watanabe, K., Izumi, K.: Central pattern generators based on matsuoka oscillators for the locomotion of biped robots. Artif. Life Robot. **12**(1-2), 264–269 (2008)
8. Inada, H., Ishii, K.: Behavior Generation of Bipedal Robot Using Central Pattern Generator (Cpg)(1St Report Cpg Parameters Searching Method by Genetic Algorithm). Intelligent Robots and Systems, 2003. (IROS 2003). Proceedings. 2003 IEEE/RSJ International Conference On, Volume 3, Pages 2179–2184. IEEE (2003)
9. Nakamura, Y., Mori, T., Sato, M., Ishii, S.: Reinforcement learning for a biped robot based on a cpg-actor-critic method. Neural Netw. **20**(6), 723–735 (2007)
10. Chen, W., Ren, G., Wang, J., Liu, D.: An adaptive locomotion controller for a hexapod robot Cpg, kinematics and force feedback. Sci. China Infor. Sci. **57**(11), 1–18 (2014)
11. Makarov, V.A., Rio, E.D., Bedia, M.G., Velarde, M.G., Ebeling, W.: Control Pattern Generator Incorporating the Actuator Dynamics for a Hexapod Robot. Int. J. Appl. Math. Comp. Sci, pages 97–102. Citeseer (2006)
12. Sabourin, C., Bruneau, O.: Robustness of the dynamic walk of a biped robot subjected to disturbing external forces by using cmac neural networks. Robot. Auton. Syst. **51**(2), 81–99 (2005)
13. Siddique, M.N.H., Tokhi, M.O.: Training Neural Networks: Backpropagation Vs. Genetic Algorithms. Neural Networks, 2001. Proceedings. IJCNN'01. International Joint Conference On, Volume 4, Pages 2673–2678. IEEE (2001)
14. Velagic, J., Osmic, N., Lacevic, B.: Neural network controller for mobile robot motion control. Int. J. Intell. Syst. Technol. Appl. **3**(2), 127–133 (2008)
15. Capi, G., Nasu, Y., Barolli, L., Mitobe, K., Takeda, K.: Application of genetic algorithms for biped robot gait synthesis optimization during walking and going up-stairs. Adv. Robot. **15**(6), 675–694 (2001)
16. Tang, Z., Zhou, C., Sun, Z.: Humanoid Walking Gait Optimization Using Ga-Based Neural Network. Advances in Natural Computation, Pages 252–261. Springer (2005)
17. Yilin, X., Gao, F., Pan, Y., Chai, X.: A Ground Contact Detection Method for a Six-Legged Robot by Motor Current. IFToMM 2015 Proceedings, Pages 275–281. IFToMM (2015)
18. Yilin, X., Gao, F., Pan, Y., Chai, X.: Method for six-legged robot stepping on obstacles by indirect force estimation. Chinese J. Mech. Eng. **29**(4), 669–679 (2016)
19. Inamura, T., Toshima, I., Tanie, H., Nakamura, Y.: Embodied symbol emergence based on mimesis theory. Int. J. Robot. Res. **23**(4-5), 363–377 (2004)
20. Pan, Y., Gao, F.: A new 6-parallel-legged walking robot for drilling holes on the fuselage Proceedings of the Institution of Mechanical Engineers, Part C: Journal of Mechanical Engineering Science, pages 753–764 (2013)
21. Yang, P., Gao, F.: Leg kinematic analysis and prototype experiments of walking-operating multifunctional hexapod robot. Proc. IME C J. Mech. Eng. Sci. **228**(12), 2217–2232 (2014)
22. Bent, L.R., Timothy Inglis, J., McFadyen, B.J.: When is vestibular information important during walking? J. Neurophysiol. **92**(3), 1269–1275 (2004)
23. Patla, A.E., Vickers, J.N.: How far ahead do we look when required to step on specific locations in the travel path during locomotion? Exp. Brain Res. **148**(1), 133–138 (2003)
24. Patla, A.E., Greig, M.: Any way you look at it, successful obstacle negotiation needs visually guided on-line foot placement regulation during the approach phase. Neurosci. Lett. **397**(1), 110–114 (2006)

25. Angelaki, D.E., Cullen, K.E.: Vestibular system: the many facets of a multimodal sense. Annu. Rev. Neurosci. **31**, 125–150 (2008)
26. Iles, J.F., Baderin, R., Tanner, R., Simon, A.: Human standing and walking: comparison of the effects of stimulation of the vestibular system. Exp. Brain Res. **178**(2), 151–166 (2007)
27. Nelson, R.J.: The somatosensory system: Deciphering the brain's own body image CRC Press (2001)
28. Chai, X., Gao, F., Pan, Y., Qi, C., Yilin, X.: A novel identification methodology for the coordinate relationship between a 3d vision system and a legged robot. Sensors **15**(4), 9519–9546 (2015)
29. Johnson, A.M., Koditschek, D.E.: Toward a Vocabulary of Legged Leaping. Robotics and Automation (ICRA), 2013 IEEE International Conference On, Pages 2568–2575. IEEE (2013)

Yilin Xu born in 1989, is currently a PhD candidate at State Key Laboratory of Mechanical System and Vibration, Shanghai, Shanghai Jiao Tong University, China. His research interests include real-time control of the legged robots.

Feng Gao born in 1956, is currently a professor at State Key Laboratory of Mechanical System and Vibration, Shanghai, Shanghai Jiao Tong University, China. His main research interests include parallel robots, design theory and its applications, large scale and heavy payload manipulator design, large scale press machine design and optimization, design and manufactory of nuclear power equipment, legged robots design and control.

Yang Pan born in 1988, received the PhD degree from Shanghai Jiao Tong University, Shanghai, China, in 2014. Then he became a postdoctoral researcher at State Key Laboratory of Mechanical System and Vibration, Shanghai Jiao Tong University, China. His research interests include design and control of legged robots.

Xun Chai born in 1990, is currently a PhD candidate at State Key Laboratory of Mechanical System and Vibration, Shanghai Jiao Tong University, China. His research interest is visual control of legged robots.